International Journal of Hydrogen Energy 73 (2024) 856–867

Contents lists available at ScienceDirect

International Journal of Hydrogen Energy

journal homepage: www.elsevier.com/locate/he

# Reforming of ammonia and ammonia-air mixtures in a homogenous plasma reactor: Parametric study of hydrogen yields

Galia Faingold *, Rany Kabour, Si Shen, Joseph K. Lefkowitz

*Technion – Israel Institute of Technology, Haifa, 3200003, Israel*

ARTICLE INFO

Handling Editor: Dr F Gallucci

*Keywords:*
Plasma assisted combustion
Plasma reforming
Ammonia cracking
Ammonia ignition
Plasma chemistry
Hydrogen energy carrier

ABSTRACT

Plasma-assisted reforming shows great promise for making ammonia compatible with current engine technology, with minimal modifications required. This study examines the impact of various discharge, flow, and composition parameters on ammonia conversion into hydrogen using a new well-stirred homogeneous plasma reactor. Gas chromatography was used to measure hydrogen and oxygen, while ICCD imaging evaluated plasma homogeneity. Initial mixture composition significantly influences the response to plasma conditions. Relative to the initial ammonia composition, the conversion of pure ammonia yields a lower hydrogen percentage when compared to air-diluted mixtures. Introducing air changes the relationship between pulsed energy deposition and hydrogen production, resulting in a more substantial increase in conversion. Efficiency calculations demonstrate that high ammonia content and high pulse frequencies improve yields, while longer residence times in the reactor result in higher temperatures, also increasing yields. These findings provide insights into the underlying mechanisms of ammonia cracking and reforming in a discharge, and will serve to promote further investigation into plasma reforming strategies.

## 1. Introduction

The 2022 United Nations Emissions Gap Report highlights the critical need to rapidly transition to renewable energy sources and adapt power production technologies accordingly, in response to the urgent demand for reducing greenhouse gas emissions [1]. One form of adaptation would be to convert fossil fuel-burning engines to run on carbon-free renewable fuels such as hydrogen or ammonia. Hydrogen production from renewable energy is currently being implemented as a method of excess energy storage. However, hydrogen is difficult and expensive to store for long periods, as well as to ship and carry on board as a fuel. Ammonia is a cheap and effective hydrogen carrier with higher volumetric energy density than liquified $H_2$ at moderate storage conditions [2–4]. The ammonia, once transported to the point-of-use location, can then be used directly as a fuel in combustion engines or in fuel cells, or be converted (in part or in full) into hydrogen for use in the same [2].

Transitioning to ammonia, however, presents its own set of challenges, particularly for combustion applications. Pure ammonia exhibits poorer combustion qualities compared to hydrocarbons, such as high NOx emissions and compatibility issues with existing engines, attributed to its low flame speed (~7 cm/s) and resistance to ignition [2]. Partial cracking of ammonia to create $NH_3/H_2$ mixtures offers a promising solution. These mixtures, especially in ratios like 70% $NH_3$/30% $H_2$, have demonstrated stable combustion in gas turbines with $NO_x$ emissions comparable to conventional fuels [2,5]. In internal combustion engines (ICEs), reforming a small portion of ammonia (<10%) can lead to stable engine performance and manageable $NO_x$ level [6]. This approach necessitates either the co-delivery and storage of hydrogen alongside ammonia or the on-site/on-board conversion of ammonia into hydrogen at the point of use, presenting new challenges and opportunities in system design and operation. For use in fuel cells, while some technologies such as solid oxide fuel cells (SOFCs) and direct ammonia fuels cells (DAFCs) can use ammonia directly, most developed devices require conversion of ammonia entirely into high purity $H_2$ before being utilized for energy production [2].

Cracking of ammonia into $H_2$ is thus required for fuel cell applications, and partial cracking also shows promise for combustion applications, particularly in achieving stable combustion and managing $NO_x$ emissions. The process of ammonia cracking itself presents a distinct set

* Corresponding author.
*E-mail address:* gfaingold@ethz.ch (G. Faingold).

https://doi.org/10.1016/j.ijhydene.2024.06.057
Received 16 April 2023; Received in revised form 14 May 2024; Accepted 5 June 2024
Available online 13 June 2024

of challenges and is a topic of ongoing research mainly in the field of catalysis [7,8]. Efficient ammonia decomposition can be achieved using various catalysts, usually at temperatures of >400 °C, generally using expensive and rare materials such as ruthenium [7] or rhodium [6]. Other catalysts, including cheaper sodium or lithium based materials, are under active development [9–11]. However, these advancements still face challenges, particularly in terms of the long-term stability of catalysts under high heat and cold-start issues in transportation, particularly if air travel is the intended application [12].

Another approach to reforming is the use of low-temperature plasma [13,14], which has the benefit of high controllability of operating conditions and no preheating necessarily required, as well as requiring no rare materials in its construction. When plasma chemical conversion is combined with catalysis, a synergistic effect generates more than the additive contribution of each separately [15,16]. While the combination of low-temperature plasma and catalysis shows potential in ammonia decomposition, a key challenge remains in achieving sufficient hydrogen yield to meet scalability and energy demand requirements, as noted in the review by Asif et al. [17]. This limitation, along with the incomplete understanding of plasma's effects on ammonia decomposition and oxidation, points to the need for innovative approaches in plasma-assisted reforming. For this, an understanding of the plasma-chemical processes in ammonia plasmas is imperative, but remains lacking.

Bridging this knowledge gap, recent research in the field of plasma-assisted combustion has begun exploring plasma discharges for the decomposition of ammonia (and ammonia-oxygen mixtures) prior to injection into a flame [18–21]. This approach, integrating an oxidizer in the plasma cracking process, offers a promising alternative to direct ammonia cracking, and is particularly relevant in applications where only moderate levels of hydrogen production are required. Previous work by Faingold et al. numerically explored plasma reforming of ammonia-air mixtures and their effect on the ensuing ignition process [18]. They found that when reforming a stoichiometric mixture of ammonia and air, a significant reduction in both ignition delay time and $NO_x$ emissions after the combustion event is possible with a limited amount of energy, due to the participation of other reforming products in the reaction processes (especially $NH_2$). A comparable reduction was possible also for a reformate of pure ammonia, for a higher energy input. It is important to note that the practicality of relying on $NH_2$ as a reforming product is dependent on its longevity and ability to be delivered to the combustor.

Further work on the development of reaction mechanisms of ammonia or ammonia-air mixtures in plasmas implemented modified versions of the model from by Faingold et al. [22] to simulate ignition and flame speed enhancement [23,24]. Taneja et al. [23] expanded the helium dilution model [22] to include nitrogen dilution, and found that an increase in pulse frequency and energy density caused a decrease in ignition delay times (IDT). This decrease in IDT was also proportional to a reduction in NO emissions. Shahsavari et al. [24], also expanding the helium model to include nitrogen dilution, showed the effect of plasma conditions and mixture composition on both ignition and flame characteristics. These findings, linking gas composition in the plasma-reforming process to the performance of a discharge, was further explored by Mao et al. [25]. In their simulation study, Mao et al. [25] found that NO production, in the pre-combustion stages, plays an important role in ignition enhancement. At fuel lean conditions, increases in O and OH production initiated by the discharge promote ignition, whereas at rich conditions the associated reactions do not. Considering these promising modeling studies, experimental efforts to collect data useful for model validation is presently ongoing by several research groups [26,27].

A recent experimental study from Cha et al. [27] on ammonia cracking in an AC dielectric barrier discharge (DBD) reactor (1 mol% of $NH_3$ diluted in $N_2$) showed cracking into hydrogen at much lower temperatures as compared to thermal decomposition, with cracking occurring even at room temperatures, and optimized at ~600 K. Interestingly, they have found non-linear behavior in which an increased gas temperature, for some plasma conditions, caused an inhibition in ammonia conversion in the presence of the plasma discharge. This was attributed to the change in reduced electric field ($E/N$) with temperature, an observation which is consistent with [24,25] where the plasma energy distribution, which is greatly dependent on the composition, changes with $E/N$.

Further exploring the effect of composition and $E/N$, Mao and coworkers [25,28,29] demonstrated how both ignition delay time and $NO_x$ respond differently to a discharge at different mixture equivalence rations. In Ref. [26], the underlying mechanism for $NO_x$ and $N_2O$ reduction under a discharge was explored, using a chemical kinetic mechanism, validated in the same study. They found that rich mixtures are preferred to lowering these emissions, as well as reducing ammonia slip. The plasma conditions themselves – $E/N$ and pulse repetition frequency – have competing effects between the creation and consumption of the different nitrogen oxides, and therefore can be optimized to yield the lowest emissions along with most complete combustion. In [29], Mao et al. numerically investigated ignition delay times under varying $E/N$ and mixture compositions. They found the discharge to be more effective in enhancing the ignition of lean mixtures, highlighting the importance of plasma-generated species created from air, and their enhancement of oxidation processes.

Although the numerical studies by Mao et al. and Zhong et al. [25,28] are based on an experimentally validated chemical kinetic model, Zhong et al.'s experimental data focused on a limited set of plasma parameters. Much of the existing experimental data has been centered on swirl-stabilized combustors, which involve either gliding arc [20,30] or nanosecond pulsed plasma [31,32] located upstream of the flame, without detailed speciation measurements in or after the discharge region. To relate the experimental findings to more in-depth chemical kinetic simulations, it is necessary to have available data with simplified physics, such as a uniform flow field and homogeneous discharge, or steady-state conditions appropriate for wide-ranging species quantification.

Addressing this need, the present study introduces a well-stirred, steady-state reactor equipped with a nanosecond pulsed DBD plasma, characterized by its homogeneity and diffuseness. This reactor is designed to generate plasma in ammonia mixtures under well-defined conditions, enabling the exploration of underlying mechanisms in plasma-ammonia interactions, aiding in the development and validation of plasma chemistry models in simplified reactor models. ICCD imaging is applied to assess the plasma's homogeneity within the reactor and to determine the operational regime, whether glow or filamentary. The study encompasses a broad range of mixtures, assessing the effects of plasma discharges on both pure ammonia (commonly used in ammonia cracking for hydrogen production) and reforming mixtures that include air (typical in plasma-assisted combustion scenarios). We investigate the influence of various parameters, including nanosecond plasma pulse repetition frequencies (PRFs), per-pulse energies, mixture residence times, and pulsed duty cycles. A key aspect of our research is quantifying the efficiency of these plasma processes, specifically measuring hydrogen yields and oxygen consumption, using ex-situ GC-TCD quantification. The insights gained from this study are aimed at enhancing understanding and informing further research in plasma reforming and cracking of ammonia with varying oxygen contents.

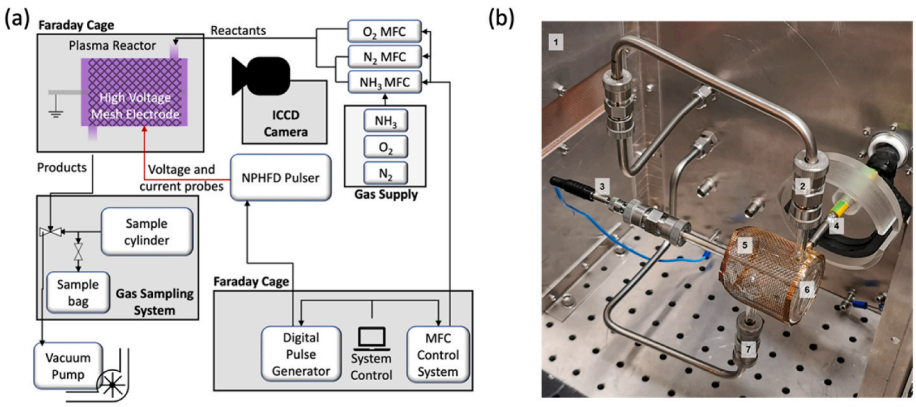


**Fig. 1.** (a) Schematic of reactor, along with controls, sampling system and optical set up. (b) The reactor assembly with enumerated components: (1) Faraday cage, (2) inlet stream, (3) ground electrode assembly, (4) high voltage electrode connector, (5) high voltage electrode, (6) quartz reactor, and (7) outlet stream.

## 2. Methods

### 2.1. Plasma reactor

Fig. 1 presents the experimental setup and reactor assembly. In Fig. 1a, we illustrate the schematic of the reactor along with its control systems, sampling setup, and optical configuration. Fig. 1b provides a detailed view of the reactor assembly with its components enumerated for clarity: (1) Faraday Cage, (2) Inlet Stream, (3) Ground Electrode Assembly, (4) High Voltage Electrode Connector, (5) High Voltage Electrode, (6) Quartz Reactor, and (7) Outlet Stream.

The reactor body, depicted schematically in Fig. 1a, is a fused silica tube measuring 4 cm in outer diameter, 5 cm in length, and with a wall thickness of 1.5 mm. The central feature of the reactor is a concentric center rod electrode configured in a double dielectric barrier setup. Specifically, the inner electrode is a 1/16″ stainless steel rod encased by an alumina dielectric tube (1/8″ outer diameter, identified as the ground electrode in Fig. 1b), and an outer mesh electrode wrapped around the exterior of the tube (marked as the high voltage electrode in Fig. 1b).

The inlet stream, which can be premixed with air, is introduced into the reactor body tangentially to the tube's axis. This design ensures rapid mixing of the reactants with the gases inside the reactor, allowing the fresh mixture to immediately interact with electrons, excited species, and radicals upon entering the reactor. This arrangement maximizes the conversion rate, in accordance to stirred-reactor theory [33]. The inlet and outlet tubes are 1/4″ fused silica which are a part of the reactor body, connected by a Swagelok Ultratorr fitting to 1/4″ stainless steel tubes passing though the Faraday Cage walls.

The discharge is created by nanosecond-duration pulsed-power generated with nanosecond-pulsed high-frequency plasma pulser (FID GmbH modified FPG 20-200NM), which has a Gaussian-shaped pulse with FWHM of 5.5 ± 0.5 ns duration, an approximate 2 ns rise time, maximum discharge voltage of 20 kV, maximum pulse repetition frequency (PRF) of up to 50 kHz for continuous pulses, or 200 kHz in burst mode. Discharge pulses were triggered using a digital delay generator (Berkeley Nucleonics Model 577). Nanosecond pulsed discharges create a non-equilibrium plasma which channels more energy into excitation and dissociation of molecules, as opposed to heating. The benefit of this discharge type is that the plasma is maintained in a non-equilibrium state despite high electric fields in the gas, allowing a significant portion of the energy to be transferred to excitation of electronic states and dissociation of molecules [34,35]. High voltage nanosecond repetitively pulsed discharges are also a popular tool for studying kinetic effects because they create uniform at low to moderate pressures discharges with exactly controllable discharge timing [34], making them ideal for imaging and spectroscopy, as well as replicating in models [36,37].

To create a volumetric discharge, the reactor is operated at a pressure of 77 Torr. The pressure control is achieved using a vacuum pump in conjunction with mass flow controllers (MFCs) for $NH_3$, $O_2$, and $N_2$. The MFCs regulate the flow rate of the gas mixture into the reactor, while a needle valve downstream of the reactor and before the vacuum pump actively maintains the reactor pressure at a steady 77 Torr. This combination ensures a consistent and controlled environment within the reactor, crucial for the stability and homogeneity of the plasma discharge.

### 2.2. ICCD imaging

In order to evaluate the plasma regime and homogeneity, emission imaging is employed, using an intensified charge coupled device (ICCD, Andor iStar DH334T with a Gen 3 HVS photocathode) paired with a UV lens (Nikon Rayfact). The camera was focused on the middle cross-section of the reactor through the round end wall. The photocathode is sensitive in the range of 280–760 nm, and no spectral filtering was utilized in the imaging. All images presented in Fig. 2 were taken with a gate time of 100 ns. Shorter gate time images (down to 4 ns) were also collected to ensure filamentary discharges were not present during the discharge. Triggering of the ICCD gate was controlled using a digital delay generator, which also triggered the nanosecond discharge, and monitored using a 1 GHz oscilloscope (Teledyne Lecroy HDO6104), ensuring that the gate timing began before and ended after a single discharge pulse. A total of 25 images were taken for each condition, at an imaging rate of 10 Hz, to ensure characteristic morphology of the discharge was observed.

### 2.3. Gas sampling

A sampling system is employed to collect gas samples for processing in a gas chromatograph with a thermal conductivity detector and mass spectrometer detector (GC-MS-TCD – ThermoFisher Scientific Trace 1300 GC), measuring hydrogen mole fraction and oxygen mole fraction

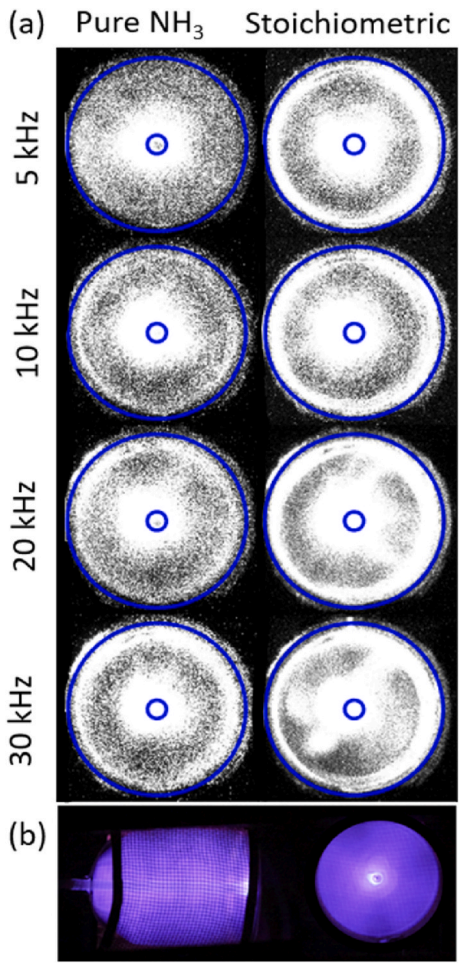


**Fig. 2.** (a) ICCD images at 20 kV and various PRFs, ans (b) the discharge in the reactor for pure nitrogen at 15 kV 10 kHz.

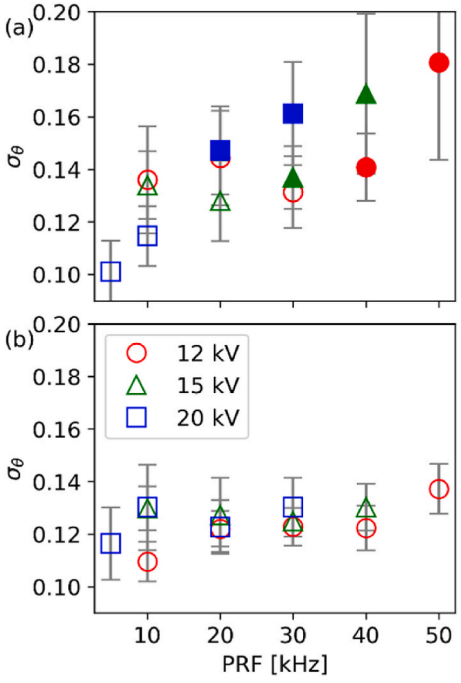


**Fig. 3.** Angular standard deviation of the intensity for (a) stoichiometric ammonia-air mixture and (b) pure ammonia. Full markers denote transitioning plasma regimes were observed.

in the exhaust gas to estimate the degree with which both pure $NH_3$ and air-diluted mixtures react. The reactor operates at 77 Torr, necessitating sample pressurization to atmospheric levels for gas chromatography (GC) analysis. Samples are collected in a pre-evacuated (<1 Torr) 2.25-liter stainless steel cylinder connected to a 1 L Tedlar Bag. After achieving reactor stability, the cylinder is filled by gradually opening a needle valve until 77 Torr is reached in the sample cylinder, after which the sample cylinder is disconnected from the reactor exhaust flow. The sample is then pressurized up to 2 bar using nitrogen, creating a dilute sample which can be released into the sample bag. The sample bag is immediately connected to the GC for analysis. The measurements only required use of the TCD sensor in the GC. These measurements are expressed as calibrated dry percentages, and the full calibration curves are given in the supplementary materials (Figs. S1S and 2S). Moisture in the effluent flow was removed using a silica gel filter element at the entrance to the sample. The minimum detectable $H_2$ mole fraction in the GC-TCD was approximately 200 ppm, leading to a measurable 3000 ppm in the experiment (considering a factor of 15 $N_2$ dilution).

### 2.4. Energy measurements and efficiency calculations

Voltage and current measurements are conducted to evaluate the average energy per pulse ($E_{PP}$) following the methods established in previous works [38–40]. The current is measured with a Rogowski coil (Magnelab CT-E2.5-BNC), and the voltage is measured using a high-voltage probe (Testec HVP 2739). These measurements were recorded on a 1 GHz oscilloscope (Teledyne Lecroy Model HDO6104). Energy measurements were performed for each plasma and dilution condition. The supplementary materials include the voltage and current measurements over a single pulse (Fig. 3S).

## 3. Results

In the course of this study, several parameters were varied to explore their effects on $H_2$ yield and conversion efficiency. These include the applied voltage, PRF, duty cycle (number of pulses per cycle – N), reactor residence time, and mixture composition. Table 1 details the range of exploration of each parameter. The following sections presents the results of each parametric study.

### 3.1. Uniformity and plasma regime estimation with ICCD imaging

Imaging with the ICCD camera is used to assess the discharge uniformity. Data was taken for pure ammonia and a stoichiometric mixture of ammonia and air, with PRFs from 2 to 50 kHz and voltages of 12, 15 and 20 kV. For each condition, 25 images were captured such that typical operation could be established.

Fig. 2a shows this behavior for several PRFs at 20 kV applied voltage: 5, 10, 20 and 30 kHz, for pure ammonia (left) and stoichiometric mixtures (right). For the pure ammonia case, the plasma distribution remains uniform, with an increase in intensity for higher PRFs. The stochiometric mixture is affected by the PRF increase, where increases in the PRF transitions the plasma from a glow discharge centered around the ground electrode, as seen in 5 kHz and 10 kHz images, to a more filamented discharge starting at 20 kHz and becoming stronger at 30 kHz. For both mixtures, the enhanced luminosity of the plasma in the central region results from a combination of emission from the cathode sheath layer around the central ground electrode and additional emission at the end of the center electrode, seen in Fig. 2b. It has also been observed that at elevated voltages, an observable sheath layer on the outer dielectric barrier is formed around the inside of the reactor

**Table 1**
Detailed summary of experimental conditions and parameters.

| Section | Varied parameter | V (kV) | PRF (kHz) | Duty cycle | $\tau$ (ms) | Mixture composition |
|---|---|---|---|---|---|---|
| 3.3.1 | Voltage and PRF | 12, 15, 20 | 10–50 | Continuous | 40 | $X_{i,NH_3} = 0.22, 1$ |
| 3.3.2 | Duty cycles | 15 | 200 | Burst frequency = 500 Hz<br>N = 20-50 | 40 | $X_{i,NH_3} = 0.22, 1$ |
| 3.3.2 | Residence time | 15 | 20 | Continuous | 40–100 | $X_{i,NH_3} = 0.22, 1$ |
| 3.3.4 | Input composition | 15 | 20, 30 | Continuous | 40 | $X_{i,NH_3} = 0.05 - 1$ |

surface, this sheath layer can be seen in Fig. 2a stochiometric mixture cases, the strongest being 20 kHz and 30 kHz.

Fig. 3 shows the standard deviation of the intensity averaged in the angular direction for 25 repeated images at each condition, as a measure of homogeneity of the plasma. An angular standard mean deviation algorithm was chosen in order to capture the variation in filamentary behavior of the plasma under different conditions. For each image, the reactor was divided in the angular direction for 360°, at each angle the intensity of the plasma was summed up, and a standard mean deviation was calculated for the angular sums by the following formula:

$$\sigma_\theta = \sqrt{\sum_{i=1}^{n} (I_\theta - \bar{I})^2 \Big/ (n-1)} \tag{1}$$

where $I_\theta$ is the total intensity at the calculated angle $\theta$, $\bar{I}$ is the averaged intensity of all angles and $n$ is the number of angles ($n = 360$). The $\sigma_\theta$ of the pure ammonia discharge is not significantly affected by the plasma conditions, and only increases slightly with PRF for the stoichiometric ammonia-air cases. This indicates that the filamentation seen in Fig. 2a is occurring randomly and infrequently, with a homogeneous plasma being the dominant discharge mode even at high PRFs.

### 3.2. Energy measurements

Table 1 shows the average $E_{PP}$ for each voltage and plasma condition, along with the standard deviation for each grouping.

$E_{PP}$ is mainly dependent on the discharge voltage and shows little variation with frequency and composition in the PRF range used in this study, as presented in Table 1. An exception is observed in the 12 kV and stoichiometric mixture case, where a combination of low energy and high noise introduces greater variance. Additionally, $E_{PP}$ was found to be independent of composition for the plasma conditions presented, with a 5% standard deviation between measured mixtures. This independence is critical as it implies that the yields from these varying mixtures, including pure ammonia and stoichiometric mixtures, can be directly compared as they result from the same energy deposition.

However, when examining plasma uniformity variation (Fig. 3), the higher variability is noted in the low-voltage stoichiometric discharge (12 kV, all PRFs), and for the 20 kV case, it only becomes significant at higher PRFs. In these scenarios, the overall energy and the signal-to-noise ratio are lower. The significance of these observations is that the differences in hydrogen yields are attributed more to the frequency of the plasma discharge rather than the $E_{PP}$, which remains consistent across various mixtures and PRFs.

### 3.3. Hydrogen production and oxygen consumption measurements

#### 3.3.1. Effect of voltage and PRF

Measurements to quantify the degree of plasma-reforming as a function of PRF and peak voltage are conducted for both pure ammonia and a stoichiometric ammonia-air mixture (22% $NH_3$/16% $O_2$/62% $N_2$), as presented in Fig. 4. The PRF is varied in the range of 2–50 kHz for voltages of 12, 15 and 20 kV. The residence time ($\tau$) of the mixture in the reactor was maintained at 40 ms, and the pressure was set to 77 Torr to enable a stable and uniform discharge. For both compositions, hydrogen is quantified in the exhaust stream, and in the stoichiometric mixture oxygen is also quantified. The hydrogen yield is determined as a percentage of the dry gas sample analyzed by the gas chromatograph (GC). To enable consistent comparisons across different gas mixtures processed in the reactor, the $NH_3$-relative $H_2$ yield, $\%H_2^*$, is defined. This is calculated as the percentage of hydrogen conversion relative to the initial ammonia mole fraction, expressed as:

$$\%H_2^* = \frac{X_{H_2}}{X_{i,NH_3}} \times 100 \tag{2}$$

where $X_{H_2}$ is the measured dry $H_2$ mole fraction in the exhaust stream and $X_{i,NH_3}$ is the $NH_3$ mole fraction in the inlet stream. $O_2$ consumption, $\%O_2^*$, is calculated as:

$$\%O_2^* = \left(1 - \frac{X_{f,O_2}}{X_{i,O_2}}\right) \times 100 \tag{3}$$

with $X_{f,O_2}$ being the measured dry oxygen mole fraction in the exhaust flow, and $X_{i,O_2}$ is the $O_2$ mole fraction in the inlet stream. For the lower PRF range, only the high voltage cases have a measurable hydrogen yield (above 5 kHz for 15 kV and 10 kHz for 12 kV). The observed range of conditions in this study is thus defined by the limitations imposed by the minimum detectable $H_2$ concentration by the GC-TCD and the maximum voltages and PRFs before arcing occurs in the reactor. Specifically, PRFs above 30 kHz (continuous) lead to arcing and temperatures exceeding the reactor's design capabilities, thereby setting the operational boundaries for our experiments.

Fig. 4 shows the measured values of $H_2$ yields and calculated $NH_3$-relative $H_2$ yield and $O_2$ consumption as a function of PRF, for varying voltages and pure and stoichiometric mixtures of ammonia. For the pure ammonia cases, the relation between PRF and hydrogen yield is close to linear, so that the hydrogen produced by the discharge is proportional to the deposited energy per unit volume, with little dependence on the rate with which energy is deposited. The involvement of air in the mixture changes this relation, so that at the higher PRFs, the hydrogen yield is growing at a faster rate as PRF is increased.

For stoichiometric mixtures in the reactor, transitions to a different plasma regime under specific conditions – namely, at 40 and 50 kHz at 12 kV, 40 kHz at 15 kV, and 10 and 20 kHz at 20 kV (indicated by full markers in Fig. 4 and subsequent figures), were observed. These transitions were characterized by periodic visible chemiluminescence, occurring much less frequently than the discharge PRF and displaying a brightness surpassing that of the non-transitioning plasma, but still

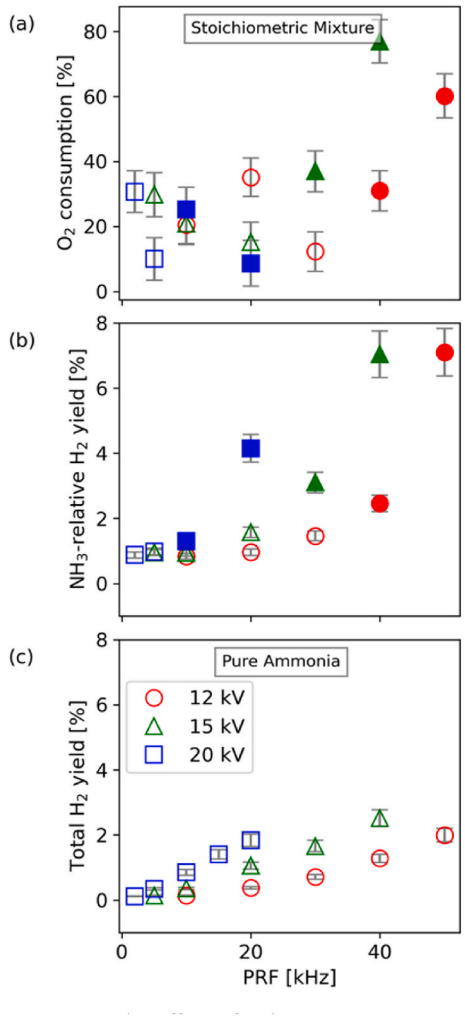


**Fig. 4.** The effect of pulse repetition frequency on (a) $O_2$ consumption, and $H_2$ production in (b) stoichiometric mixtures and (c) pure ammonia. Full markers denote transitioning plasma regimes were observed.

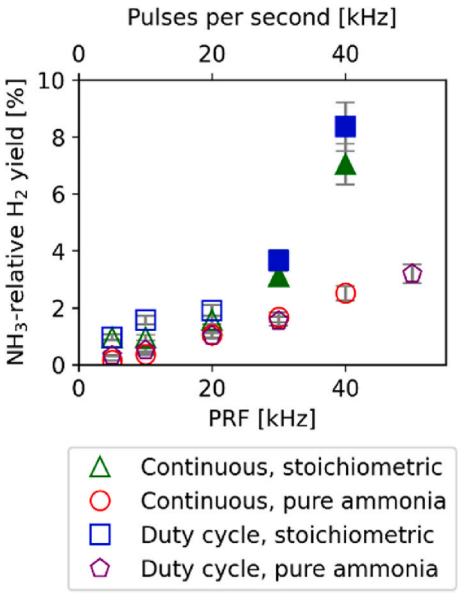


**Fig. 5.** The effect of 200 kHz bursts at 15 kV on hydrogen yields, compared to corresponding cases at continuous pulsing mode and lower PRFs. Full markers denote transitioning plasma regimes were observed.

being relatively diffuse according to ICCD imaging. The occurrences, suggestive of localized ignition events, were brief yet distinct. Oxygen consumption measurements, showing an increased consumption particularly for the highest PRF cases (40 kHz at 15 kV and 50 kHz at 12 kV), corroborate these observations, though complete oxygen consumption was not achieved. This is attributed to the transient nature of these plasma regime transitions, coupled with the extended duration (several seconds) of product sample collection. Notably, conditions proximate to these plasma regime transitions resulted in relatively high $H_2$ yields, hinting at potential operational benefits near this threshold, such as the 20 kHz, 20 kV condition. Further investigations, including comprehensive species measurements, are essential to thoroughly characterize the reformate composition and understand these plasma phenomena.

### 3.3.2. *Effect of pulse bursts at high PRF*

To further investigate the effect of pulse deposition rates, a comparison is made between continuously pulsed cases and pulses deposited at a PRF of 200 kHz (the maximum possible from the pulsed power supply) at duty cycles with repeating bursts. Fig. 5 shows the $NH_3$-relative hydrogen yields at 15 kV peak voltage and continuous PRFs ranging from 5 to 40 kHz, and a corresponding case with the same number of pulses deposited per second. In burst mode, the total number of pulses deposited per second matches that of the continuous mode by employing bursts of N = 20–80 pulses at a 200 kHz PRF, with a burst repetition frequency set at 500 Hz. For the pure ammonia cases, there is no measurable difference in hydrogen yield between continuously pulsed and duty cycle cases, indicating that at even higher frequencies, there is no beneficial pulse-to-pulse build up effects. However, for the stoichiometric cases, we again observe a non-linear increase in hydrogen yields with PRF, which is slightly accentuated in duty cycle mode.

At the highest pulse numbers N = 60–80 pulses per burst at 200 kHz, equivalent to 30 and 40 kHz continuous pulsing, respectively, a steady and repeatable flickering was observed, suggesting a transition to a different plasma state after a certain number of bursts. The steady flickering could indicate ignition after a set number of bursts. This may be a similar phenomenon to what was observed in Refs. [39,40], where discharge bursts first build a radical pool, followed by a forced ignition at a critical burst number. Further investigations measuring species and temperature in the reactor are necessary to characterize these events as ignition or an instability in the plasma itself.

### 3.3.3. *Effect of residence time*

Fig. 6 presents the effect of residence time on hydrogen production under a 15 kV and 20 kHz discharge. Under these conditions, the discharge is uniform, and the stoichiometric mixture remains in the homogeneous regime (see Fig. 4, $O_2$ consumption). For the pure ammonia case (blue squares), the increasing residence time results in a moderate, linear rise in $H_2$ yields at $\tau = 40 - 70$ ms, but going from 70 to 80 ms there is a sharp increase. At $\tau = 80$ ms, the converted $H_2$ is 3.4%, an increase of more than three-fold when compared to half the residence time (40 ms, 1.05%). The maximum $H_2$ yield is 5.11%, reached at 100 ms residence time, which is the highest absolute $H_2$ yield found in this study. The stoichiometric case (red circles) exhibits a close to linear increase throughout the residence time range. The greatest $NH_3$-relative $H_2$ yield for the stoichiometric condition is 5.43%, slightly greater than the pure ammonia condition.

Increasing the residence time in the stoichiometric mixture to $\tau = 80$ ms with 15 kV and 20 kHz plasma conditions yields a similar amount of hydrogen as the 15 kV and 30 kHz PRF case with $\tau = 40$ ms, but in the latter conditions a transition in the plasma regime was observed. This is

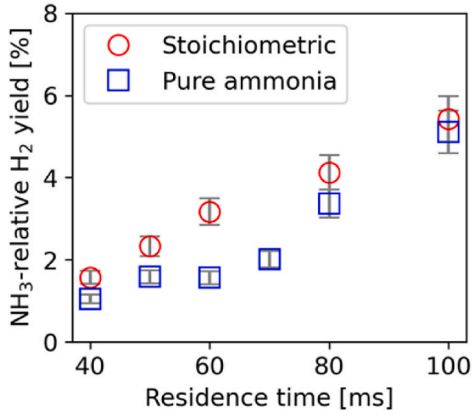


**Fig. 6.** The effect of residence time on hydrogen yields, for 15 kV pulses at a PRF of 20 kHz, for pure ammonia and a stoichiometric mixture.

despite a greater plasma energy exposure during the longer residence time in the former case (1600 pulses compared to 1200 pulses), indicating that the transitioning plasma regime is mainly determined by a critical intensity of plasma conditions.

### 3.3.4. *Effect of mixture composition*

Fig. 7 shows oxygen consumption (a) and the hydrogen yields (b) for two plasma conditions, PRFs of 20 and 30 kHz and 15 kV peak voltage, with air dilution ranging from 0 to 95% ($X_{NH3,i} = 0.05 - 1$). Due to the relatively low voltage and PRF, these are all non-transitioning cases. Because of the wide range of initial ammonia content, the absolute values of hydrogen yields are also included in the plot (c), to give a sense of the overall conversion. The highest $NH_3$-relative $H_2$ yield occurs for very high dilution rates, reaching 6.5% $H_2$ created from the initial $NH_3$ concentration, for the case of 30 kHz PRF. While as a relative value it is a very high yield, the absolute value is only 0.33% $H_2$ in the reacted mixture. With increasing ammonia fractions, the decrease in relative conversion and increase in absolute $H_2$ yield are almost monotonous. There is a slight dip in the plot around 22% ammonia, which may be due to a tendency to consume hydrogen around the stoichiometric mixture.

Oxygen consumption trends differ from very lean to very rich mixtures. For the lean-stoichiometric cases, there is an initial decrease of consumption, followed by a rapid increase of consumption around stoichiometry. At rich conditions, after stoichiometric and up to 80%/20% $NH_3$/air, oxygen consumption levels remain steady, indicating that it is possible to convert ammonia into a useful mixture and without fully consuming the $O_2$ in rapid reactions. At the very small dilution proportions, nearly all of the oxygen is consumed. Since it is a small amount initially, the effect on conversion to useful mixtures is negligible.

## 4. Discussion

Measurements of hydrogen yields under varying PRF (Fig. 4) showed that in pure ammonia, hydrogen output linearly correlates with energy input, whereas in mixtures with air, higher PRFs significantly increase hydrogen production. In examining the conversion of pure ammonia, it is crucial to consider the role of electron-collision reactions. These reactions, primarily involving $NH_3$, are central to understanding the linear trend of $H_2$ formation with respect to PRF. This reflects similar findings in the simulation study by Faingold et al. [18], where pure ammonia under a discharge was converted at a rate that was directly proportional to the number of pulses deposited (equivalent to the energy input), while stoichiometric mixtures had additional reactions that enhanced conversion in-between pulses. For pure ammonia conversion, the main consumption reactions for $NH_3$ in the plasma are [18,22,27]:

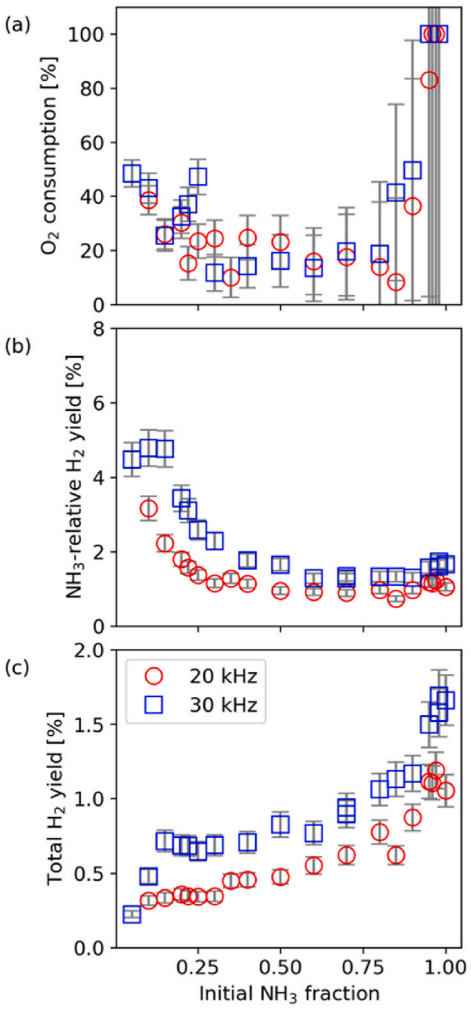


**Fig. 7.** The effect of composition on (a) oxygen consumption and (b) relative and (c) absolute hydrogen yields. Plasma conditions are 15 kV and 20 and 30 kHz PRF.

(R1) $NH_3 + e^- \rightarrow NH_2 + H + e^-$

(R2) $NH_3 + e^- \rightarrow NH + 2H + e$

Likely, the reaction with electronically-excited $N_2$ is playing a secondary role (due to low concentrations of $N_2$):

$NH_3 + N_2^* \rightarrow NH_2 + H + N_2^{*-1}$

Here, $N_2^*$ refers to the electronically excited states $N_2$ ($A^3\ \Sigma_u^+$), $N_2(B^3\ \Pi_g)$, $N_2(B'^3\ \Sigma_u^-)$, $N_2(W^3\ \Delta_u)$, $N_2$ ($a'^1\ \Pi_g$), $N_2$ ($w^1\ \Delta_u$) and $N_2(C^3\ \Pi_u)$, and $N_2^{*-1}$ is a reduced energy state compared to the one on the left-hand side of the reaction. The H atom formed in these reactions can then proceed to react with ammonia via:

$NH_3 + H \rightarrow NH_2 + H_2$

or recombine with other H atoms to produce the measured $H_2$. Reactions with hydrazine ($N_2H_4$) and associated species play a secondary role according to the analysis by Bang et al. [27]. Each electron-collision that dissociates $NH_3$ produces one $H_2$ molecule, accounting for the linear trend of $H_2$ formation with PRF.

In stoichiometric mixtures, hydrogen yield trends exhibit non-linearity (Fig. 4). In examining the effects of voltage and PRF, when

viewed alongside the $O_2$ consumed in the reactor, it is apparent that there are underlying and competing mechanisms that produce and consume hydrogen in the stoichiometric mixture. Unlike $H_2$ yields, which increase with PRF for a constant applied voltage, there are no clear trends in oxygen consumption for the low PRF cases (homogeneous plasma regime, open symbols in Fig. 4). Higher PRFs lead to both increased oxygen consumption but also increased hydrogen production. The persistence of hydrogen as a product in more completely reacted mixtures (based on oxygen consumption) is noteworthy. If there is a critical conversion degree that causes localized ignition, in which the fresh mixture must be exposed to the plasma for some amount of pulses before ignition, it will cause the ignited mixture, in which $O_2$ and $H_2$ were consumed, to mix with an unignited one. The transition to a different plasma regime along with the local ignition likely leads to near-adiabatic flame temperature for short periods of time, so even when returning to a diffuse plasma regime high rates of reforming may be present due to the high temperature. This is analogous to hydrogen production observed in the post-flame region of superadiabatic flames [41], and the conversion quantities measured here are within the reported range of hydrogen in these flame simulations [42]. Further studies will measure the frequency and duration of plasma regime transitions, along with species such as $H_2O$, NO and $NH_2$ will be able to assess whether this is ignition phenomena, and how much of the sample composition are combustion products, versus unburned reformates.

In burst mode, hydrogen yields were compared to the equivalent cases in continuous pulsing mode. The linear trends of hydrogen yield for the pure ammonia conversion are preserved when pulsing at burst mode (Fig. 5), and yield percentages which closely follow those of the continuous cases. This further strengthens the claim that for pure ammonia, the rate of pulse deposition and the $E_{PP}$ are not independently the driving factors for conversion, and the amount of energy deposited overall into the same gas volume is the driving parameter, as most of the dissociation is initiated directly from electron collisions during the discharge itself [22]. The stoichiometric case shows more conversion for burst mode when compared to continuous pulsing, in both the homogeneous plasma regime and the transitioning plasma regime. In Ref. [18], reforming simulations demonstrated that for longer residence times, temperature increases and the overall decomposition increases due to higher production rates of OH and $HO_2$ resulting from the H initially formed in (R1) and (R2). Considering the homogeneous plasma case, according to numerical simulations performed at similar conditions [18], and in accordance with the measurements of $NH_3$ consumption as a function of temperature in the work of Bang et al. [27], both $H_2$ selectivity and overall $NH_3$ consumption increase with reactor temperature, which they attribute both to changes in $E/N$ with $T_g$ and the competition between chain branching and chain terminating reactions. In burst mode cases, the local temperature is expected to be greater than in continuously pulsed cases, which would lead to greater $H_2$ yields.

As the residence time is increased, as explored in Section 3.3.3, the average energy deposited into the gas increases, and thus a linear increase in the hydrogen yield is expected. A useful comparison can be made by defining a specific energy input (SEI):

$$\mathrm{SEI(J/mL)} = \frac{\text{Plasma power}}{\text{Total feed flow rate}} = \frac{\mathrm{PRF} \times E_{pp} \times V}{Q_{\mathrm{tot}}} \tag{4}$$

where $V$ is the volume of the reactor and $Q_{\mathrm{tot}}$ is the volumetric flow rate into the reactor. Fig. 8 shows the hydrogen yields as a function of SEI for all the parametric exploration in Sections 3.3.1–3.3.3, for both the stoichiometric case (Fig. 8a) and the pure ammonia cases (Fig. 8b).

Considering the pure ammonia cases first, a nearly linear increase in $H_2$ yield is found with SEI, with little variance between cases at different $E_{pp}$, PRF, $\tau$, or using duty cycles. This reinforces the concept that the $H_2$ production is governed mainly by electron collision reactions, where any method of increasing SEI leads to increased yields. There is some variation amongst different conditions, particularly at SEI $>$ 0.3, for example the long residence time cases have greater $H_2$ yield than other conditions. Further measurements will elucidate these differences.

In stoichiometric mixtures, there is also a linear increase in relative $H_2$ yields with SEI (Fig. 8a), with only 3 points as outliers. The outlier conditions are all occurring in the transitioning plasma conditions, for conditions of (1) 12 kV, 50 kHz, (2) 15 kV, 40 kHz, and (3) burst mode at 15 kV and equivalent PRF of 40 kHz. All other cases, including ones which were identified as being within the transitioning plasma regime, fall along a conversion trend very similar to the pure ammonia cases. Interestingly, this includes SEI conditions greater than those leading to localized ignition, indicating that the plasma transition is not a direct function of SEI. For example, the longest residence time condition maintained with plasma generated at peak voltage of 15 kV and PRF of 20 kHz, resulted in a homogeneous plasma and SEI of 0.38 J/mL. The relative $H_2$ yield for this case is 5.4%, which is about the same as in the pure ammonia case for the same plasma condition, which had an $H_2$ yield of 5.1%. It was also noted in Ref. [18] that conditions which are near to ignition produce the highest hydrogen yields. This is perhaps an example of a case where the ignition threshold is approached but never reached in a continuous fashion, and thus relatively high hydrogen production is reached even without a transition in the plasma regime linked to localized ignition.

As demonstrated in the comparisons of pure ammonia conversion to that of a stoichiometric mixture, the effect of composition is crucial to conversion (Fig. 7). Operating under lean conditions (initial $NH_3$ fraction less than 0.22), the $NH_3$-relative $H_2$ yield is highest, but because it is a small overall amount of ammonia, the total H2 yield is low. For rich conditions, the $NH_3$-relative $H_2$ yield is almost constant, but the total $H_2$ yield increases significantly. For very small dilution proportions (above 70% ammonia), there is a small increase in relative hydrogen production accompanied by a rapid increase in total $H_2$ yield as the initial $NH_3$ fraction is increased. For some case above 90% initial $NH_3$ fraction, there is superior yield than in the pure ammonia case, which indicates that this may be an optimal mode to operate, with a small amount of air enhancing conversion without consuming the produced $H_2$, a hypothesis which will be examined in further studies.

To determine the overall optimum operating conditions, the efficiencies of conversion to hydrogen were calculated for all hydrogen yields explored in Section 3.3, using current and voltage measurements,

$$E_{H2} = C_{H2} \bullet \frac{Q_{tot}}{P_{tot}} = \frac{C_{H2}}{SEI}, \tag{5}$$

which has units of $g/kWh$. Here. $C_{H2}$ is the hydrogen concentration coming out of the reactor in g/cm$^3$, $Q_{tot} = V_{reactor}/\tau$ is the volumetric flow rate in the reactor and $P_{tot} = E_{pp} \bullet PRF \bullet V_{reactor}$ is the total power input for each plasma condition. The efficiency formula can also be interpreted as the ratio of hydrogen concentration to the specific energy input, which is calculated as the total power input divided by the total flow rate (Eq. (4)). Efficiency for all conditions is summarized in Fig. 9. In Fig. 9a, representing stoichiometric mixtures at varying peak voltage and PRF conditions, efficiency for the lowest power cases (lowest PRF at each peak voltage) peaks at approximately 2 g/kWh, with a steady reduction in efficiency as PRF is increased up until the cases that show transitioning in the plasma regime. While the transitioning cases do

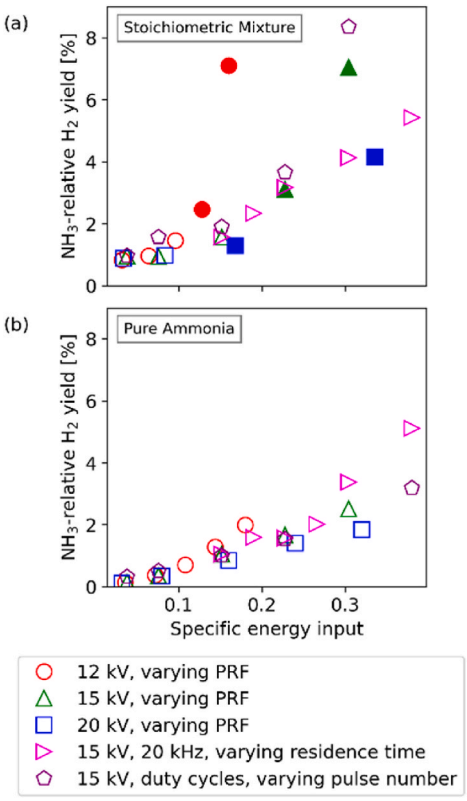


**Fig. 8.** The effect of specific energy input on the hydrogen yields for the different plasma and residence time conditions, for (a) stoichiometric mixtures and (b) pure ammonia. Full markers denote transitioning plasma regimes were observed.

show an increase in efficiency with PRF, it should be noted that the efficiency only considers the absolute concentration of $H_2$ in the reformate stream, without considering how much of the $NH_3$ is oxidized to $H_2O$, which is a relatively large percent as evident from the amount of oxygen consumption (Fig. 4a). Efficiency for those air-diluted cases are thus difficult to directly compare to other conditions.

In Fig. 9d, for pure ammonia cases at varying peak voltage and PRF, there is a linear increase in efficiency with PRF, without much variance among the different voltage conditions. This indicates that the conversion efficiency is not a function of $E_{pp}$, for the range of $E_{pp}$ = 0.09–0.4 mJ/cm$^3$, which is in line with the assertion that the amount of $NH_3$ conversion is directly proportional to the electrical energy deposited. However, the trend of increasing conversion efficiency with PRF leads to a different conclusion, indicating that the $H_2$ yield is a function of PRF (independently from SEI), perhaps due to increasing temperature in the reactor. At low PRFs (2-10 kHz) in the pure-ammonia cases, some efficiencies are lower than those of the stoichiometric mixtures, for instance at 20 kV and 2 kHz, $E_{H2}$ = 1.05 and 1.72 g/kWh for pure and stoichiometric cases, respectively, while for PRF ≥20 kHz, the efficiency is greater for the pure ammonia cases. In Fig. 4, the hydrogen yields were normalized to show the relative conversion, while calculations of efficiency were done with absolute values, to reflect the overall power that is applied to produce $H_2$. When viewed from the perspective of efficiency of conversion to $H_2$, pure and very rich ammonia reforming has significantly higher yield and $E_{H2}$ compared to stoichiometric or significantly diluted cases (Fig. 9f).

Fig. 9b and e presents $E_{H2}$ as a function of the number of pulses deposited per second for the conditions explored in Section 3.3.2, comparing continuous and duty-cycle operating modes. For the stoichiometric mixtures, similar to in Fig. 9a, the efficiency of conversion of stoichiometric mixtures steadily reduces as the effective PRF is increased, until the plasma transition is reached. In the pure ammonia conversion cases of Fig. 9e, there is an advantage of operating in duty cycles for low pulse numbers (less than 20 kHz) which is not apparent for higher PRFs. This is possibly again due to higher temperatures in the pulse burst aiding conversion, while continuous low frequency pulsing does not result in similar temperature increases. This difference is negated for PRF ≥20 kHz.

For longer residence times (Fig. 9c) there is a steady increase of hydrogen yields for stoichiometric mixtures (Section 3.3.4 and Fig. 6), but efficiency remains steadily low at $E_{H2} \approx 0.9$ g/kWh. However, the $E_{H2}$ continually increases for the pure ammonia cases, reaching approximately 4 g/kWh at $\tau$ = 100 ms, the highest found of any condition. It is notable that this condition also resulted in the greatest overall $H_2$ conversion (see Fig. 6), indicating that long residence time, pure ammonia reforming results in both the highest yield and highest efficiency in the study. As discussed in Faingold et al. [18], this is likely a result of operating near but below the ignition condition for extended periods of time.

Varying air dilution (Fig. 9f) shows a trend of increasing $E_{H2}$ with increasing initial $NH_3$ fraction (none of the mixtures ignite under the selected plasma conditions). However, over a large range of mixture fractions, e.g. $X_{NH3,i}$ = 0.1–0.8, $E_{H2}$ remains almost constant, increasing gradually for $X_{NH3,i} > 0.8$, indicating that the presence of an oxidizer even in relatively low concentrations negatively impacts $H_2$ conversion efficiency. This is likely due to a balance between $H_2$ and $H_2O$ production pathways, with the latter reaction path impeding $H_2$ production until the air dilution percentage is very low. However, in our previous study [18], it was noted that some oxidation products can enhance ignition in the reformed mixtures, and thus the optimal mixture fraction for reforming considering all ignition-promoting species must be evaluated after a wider range of species is measured.

Based on the efficiency of $H_2$ production and the overall yields, it is evident that pure ammonia reforming with a high PRF plasma and long residence time results in the optimal operating condition for the present DBD reactor. While this result is unsurprising when considering only $H_2$ yield, the increased efficiency at these conditions indicates a non-linear behavior of $NH_3$ conversion which coincides with conditions corresponding to high-temperature operation, suggesting an optimum in which a synergy between thermal decomposition and plasma chemistry occurs [27].

In the work by Andersen et al. [16], they utilize a value η, akin to our hydrogen yield efficiency $E_{H2}$, but based on the ammonia consumption measured post-reactor. For pure ammonia reforming, it is possible to compare our results, using,

$$\eta(\%) = \frac{X_{NH3} \bullet \Delta_r H}{SEI \bullet \rho_{NH3} \bullet M_{NH3}}, \quad (6)$$

with $\Delta_r H$ being the reaction enthalpy, taken as 16.8 J/ml, $X_{NH3}$ is the final ammonia fraction, calculated based on the hydrogen output measurements and assuming only hydrogen, nitrogen and ammonia in the final mixture, and $\rho_{NH3}$ and $M_{NH3}$ being the ammonia concentration and mass, respectively. Comparing the results from Andersen's study to the present study, they had kept the SEI at a constant level of 16.8 J/ml, in comparison to a range of 0.15-1.6 J/ml in the current study. This order of magnitude difference is due to the relatively low pressures which

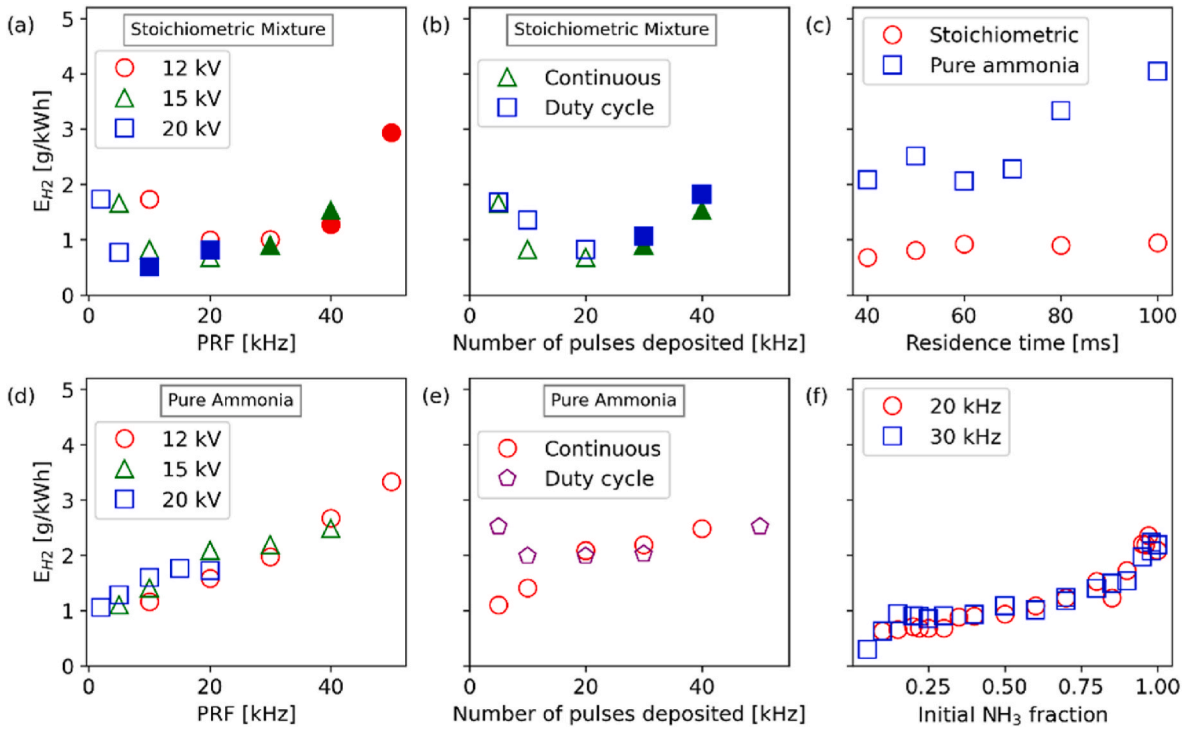


**Fig. 9.** Hydrogen yield efficiency for (a) stoichiometric mixtures under varying PRFs and discharge voltages, (b) stoichiometric mixtures under duty cycles at 15 kV and 200 kHz PRF, (c) varying residence time at 15 kV and PRF of 20 kHz, (d) pure ammonia under varying PRFs and discharge voltages, (e) pure ammonia under duty cycles at 15 kV and 200 kHz PRF, and (f) varying mixture compositions at 15 kV and PRFs of 20 and 30 kHz. Full markers denote transitioning plasma regimes were observed.

enable low plasma power, typical of nanosecond pulsed plasma operation. The value of η, however, is normalized by SEI, enabling a direct comparison of hydrogen yields. Comparing those values, for plasma only, Anderson et al. had an efficiency of $\eta = 0.38\%$, and reached peak efficiency of $\eta = 1.73\%$, with a $MgAl_2O_4$ catalyst. In the present study, the maximum efficiency η for pure ammonia conversion was $\eta = 1.48\%$ for the high PRF case (12 kV and 50 kHz), with other efficiencies ranging being slightly lower but comparable, as discussed in previous paragraphs. While direct comparisons are challenging due to Andersen's experiments being conducted using different plasma types, pressures and flow rates, and using catalysts, the trends still hold promise for achieving significant hydrogen yields without the need for catalysts.

## 5. Conclusions

The present work demonstrates the effect of different discharge, flow and composition parameters on ammonia conversion in a well-stirred plasma reactor. Hydrogen measurements were performed by GC-TCD sampling of the product stream, and showed that the initial mixture composition largely influences the sensitivity to pulse repetition frequency, with a transition to a non-uniform plasma regime apparent in only stoichiometric cases, indicating a feedback with heat release from combustion reactions [43]. The total $H_2$ conversion rate (for pure ammonia) and $NH_3$-relative $H_2$ conversion rate (for stoichiometric cases) was found to increase with specific energy input monotonically. When conversion is normalized by SEI, only the PRD and not the $E_{pp}$ was found to influence conversion efficiency. It was also found that the efficiency of $H_2$ production is maximized for pure ammonia reforming, with high PRF and residence times maximizing both total yield of $H_2$ and $E_{H2}$.

Previous studies found benefits of ammonia reforming before injection into engines, such as ignition enhancement and $NO_x$ reduction were possible at the addition of just 0.8% of hydrogen if it is combined with other reformates such as amino radicals, given they are produced close enough to the combustion application to remain active [18]. The conversion achieved in this experimental study, especially for reforming pure mixtures, shows that this is achievable at moderate plasma conditions. Yields can be enhanced for rich ammonia-air mixtures, and those can be mixed into an engine intake stream to achieve more efficient combustion at overall lean or stoichiometric conditions.

These findings lay the groundwork for future research into the intricate mechanisms underlying the observed plasma behaviors and conversion patterns. Expanding the dataset to include temperature profiles and additional intermediate species will be crucial for developing a comprehensive chemical kinetic model that can accurately capture the dynamics of plasma-assisted processes. This initial study demonstrates that reforming with a nanosecond repetitively pulsed discharge in a DBD configuration at low initial temperatures and pressures can yield up to 10% hydrogen. Incorporating plasma catalysis into this process shows potential for further enhancing these yields [44]. Additionally, exploring the addition of oxygen to the reformed mixtures could open new pathways for efficiency improvements, especially in the context of plasma-enhanced reforming techniques. Such hybrid approaches, combining plasma with catalysis and optimal oxygen levels, could significantly advance the effectiveness of ammonia reforming for hydrogen production.

## CRediT authorship contribution statement

**Galia Faingold:** Conceptualization, Data curation, Formal analysis, Funding acquisition, Investigation, Methodology, Project administration, Resources, Software, Supervision, Visualization, Writing – original draft, Writing – review & editing. **Rany Kabour:** Data curation, Formal analysis, Writing – original draft, Software. **Si Shen:** Data curation, Formal analysis, Methodology, Software. **Joseph K. Lefkowitz:** Conceptualization, Data curation, Formal analysis, Funding acquisition, Methodology, Supervision, Writing – original draft, Writing – review & editing, Project administration, Resources.

## Declaration of competing interest

The authors declare that they have no known competing financial interests or personal relationships that could have appeared to influence the work reported in this paper.

## Acknowledgements

The authors would like to thank Doral Group Renewable Resources, Ltd for their support, as well as the Binational Science Foundation for their support under NSF-BSF grant number 2022661. We also extend our gratitude to Dr. Bret Windom and Dr. Azer Yalin at Colorado State University, who collaborated with us through the NSF-BSF Foundation.

## Abbreviations

| | |
|---|---|
| IDT | ignition delay time |
| ICE | internal combustion engines |
| PRF | pulsed repetition frequency |
| $E_{pp}$ | energy per pulse |
| DBD | dielectric barrier discharge |

## Appendix A. Supplementary data

Supplementary data to this article can be found online at https://doi.org/10.1016/j.ijhydene.2024.06.057.

## References

[1] United Nations Environment Programme. Emissions gap Report 2022: the closing window — climate crisis calls for rapid transformation of societies. 2022. Nairobi.
[2] Valera-Medina A, Amer-Hatem F, Azad AK, Dedoussi IC, De Joannon M, Fernandes RX, et al. Review on ammonia as a potential fuel: from synthesis to economics. Energy Fuel 2021;35:6964–7029. https://doi.org/10.1021/acs.energyfuels.0c03685.
[3] Palys MJ, Wang H, Zhang Q, Daoutidis P. Renewable ammonia for sustainable energy and agriculture: vision and systems engineering opportunities. Curr Opin Chem Eng 2021;31:100667. https://doi.org/10.1016/J.COCHE.2020.100667.
[4] Valera-Medina A, Xiao H, Owen-Jones M, David WIF, Bowen PJ. Ammonia for power. Prog Energy Combust Sci 2018;69:63–102. https://doi.org/10.1016/J.PECS.2018.07.001.
[5] Kobayashi H, Hayakawa A, Somarathne KDKA, Okafor EC. Science and technology of ammonia combustion. Proc Combust Inst 2019;37:109–33. https://doi.org/10.1016/j.proci.2018.09.029.
[6] Koike M, Miyagawa H, Suzuoki T, Ogasawara K. Ammonia as a hydrogen energy carrier and its application to internal combustion engines. Inst Mech Eng – Sustain Veh Technol Driv Green Agenda 2012:61–70. https://doi.org/10.1533/9780857094575.2.61.
[7] Inamuddin Boddula R, Asiri AM, editors. Sustainable ammonia production. Springer International Publishing; 2020.
[8] Nagaoka K, Eboshi T, Takeishi Y, Tasaki R, Honda K, Imamura K, et al. Carbon-free H2 production from ammonia triggered at room temperature with an acidic RuO2/γ-Al2O3 catalyst. Sci Adv 2017;3. https://doi.org/10.1126/SCIADV.1602747/SUPPL_FILE/1602747_SM.PDF.
[9] Makepeace JW, Wood TJ, Hunter HMA, Jones MO, David WIF. Ammonia decomposition catalysis using non-stoichiometric lithium imide. Chem Sci 2015;6:3805–15. https://doi.org/10.1039/C5SC00205B.
[10] David WIF, Makepeace JW, Callear SK, Hunter HMA, Taylor JD, Wood TJ, et al. Hydrogen production from ammonia using sodium amide. J Am Chem Soc 2014;136:13082–5. https://doi.org/10.1021/JA5042836/SUPPL_FILE/JA5042836_SI_001.PDF.
[11] Wood TJ, Makepeace JW, Hunter HMA, Jones MO, David WIF. Isotopic studies of the ammonia decomposition reaction mediated by sodium amide. Phys Chem Chem Phys 2015;17:22999–3006. https://doi.org/10.1039/C5CP03560K.
[12] Otto M, Vesely L, Kapat J, Schmitt J. Challenges and opportunities of ammonia as a zero-emission aircraft. Fuel 2024. https://doi.org/10.2514/6.2024-0739.
[13] Snoeckx R, Bogaerts A. Plasma technology – a novel solution for CO 2 conversion? Chem Soc Rev 2017;46:5805–63. https://doi.org/10.1039/C6CS00066E.
[14] Adamovich I, Agarwal S, Ahedo E, Alves LL, Baalrud S, Babaeva N, et al. The 2022 Plasma Roadmap: low temperature plasma science and technology. J Phys D Appl Phys 2022;55:373001. https://doi.org/10.1088/1361-6463/AC5E1C.
[15] Bogaerts A, Tu X, Whitehead JC, Centi G, Lefferts L, Guaitella O, et al. The 2020 plasma catalysis roadmap. J Phys D Appl Phys 2020;53:443001. https://doi.org/10.1088/1361-6463/ab9048.
[16] Andersen JA, Christensen JM, Østberg M, Bogaerts A, Jensen AD. Plasma-catalytic ammonia decomposition using a packed-bed dielectric barrier discharge reactor. Int J Hydrogen Energy 2022;47:32081–91. https://doi.org/10.1016/J.IJHYDENE.2022.07.102.
[17] Asif M, Sidra Bibi S, Ahmed S, Irshad M, Shakir Hussain M, Zeb H, et al. Recent advances in green hydrogen production, storage and commercial-scale use via catalytic ammonia cracking. Chem Eng J 2023;473:145381. https://doi.org/10.1016/J.CEJ.2023.145381.
[18] Faingold G, Kalitzky O, Lefkowitz JK. Plasma reforming for enhanced ammonia-air ignition: a numerical study. Fuel Commun 2022;12:100070. https://doi.org/10.1016/J.JFUECO.2022.100070.
[19] Choe J, Sun W, Ombrello T, Carter C. Plasma assisted ammonia combustion: simultaneous NOx reduction and flame enhancement. Combust Flame 2021;228:430–2. https://doi.org/10.1016/j.combustflame.2021.02.016.
[20] Lin Q, Jiang Y, Liu C, Chen L, Zhang W, Ding J, et al. Controllable NO emission and high flame performance of ammonia combustion assisted by non-equilibrium plasma. Fuel 2022;319:123818. https://doi.org/10.1016/J.FUEL.2022.123818.
[21] Choe J, Sun W. Experimental investigation of non-equilibrium plasma-assisted ammonia flames using NH2* chemiluminescence and OH planar laser-induced fluorescence. Proc Combust Inst 2022. https://doi.org/10.1016/j.proci.2022.07.001.
[22] Faingold G, Lefkowitz JK. A numerical investigation of NH3/O2/He ignition limits in a non-thermal plasma. Proc Combust Inst 2021;38:5849–57. https://doi.org/10.1016/j.proci.2020.08.033.
[23] Taneja TS, Johnson PN, Yang S. Nanosecond pulsed plasma assisted combustion of ammonia-air mixtures: effects on ignition delays and NOx emission. Combust Flame 2022;245:112327. https://doi.org/10.1016/J.COMBUSTFLAME.2022.112327.
[24] Shahsavari M, Konnov AA, Valera-Medina A, Jangi M. On nanosecond plasma-assisted ammonia combustion: effects of pulse and mixture properties. Combust Flame 2022;245:112368. https://doi.org/10.1016/J.COMBUSTFLAME.2022.112368.
[25] Mao X, Zhong H, Liu N, Ju Y. Ignition enhancement of NH 3/air mixtures by non-equilibrium excitation in a nanosecond pulsed plasma discharge. In: AIAA SCITECH 2023 Forum; 2023. https://doi.org/10.2514/6.2023-0748.
[26] Zhong H, Mao X, Liu N, Wang Z, Ombrello T, Ju Y. Understanding non-equilibrium N2O/NOx chemistry in plasma-assisted low-temperature NH3 oxidation. Combust Flame 2023;256:112948. https://doi.org/10.1016/J.COMBUSTFLAME.2023.112948.
[27] Bang S, Snoeckx R, Cha MS. Kinetic study for plasma assisted cracking of NH3: approaches and challenges. J Phys Chem A 2023;127:1271–82. https://doi.org/10.1021/ACS.JPCA.2C06919/SUPPL_FILE/JP2C06919_SI_002.ZIP.
[28] Zhong H, Liu N, Mao X, Wang Z, Ju Y. Kinetic studies of low-temperature ammonia oxidation in a nanosecond repetitively-pulsed discharge. In: AIAA SCITECH 2023 Forum; 2023. https://doi.org/10.2514/6.2023-1694.
[29] Mao X, Zhong H, Liu N, Wang Z, Ju Y. Ignition enhancement and NOx formation of NH3/air mixtures by non-equilibrium plasma discharge. Combust Flame 2024;259:113140. https://doi.org/10.1016/J.COMBUSTFLAME.2023.113140.
[30] Tang Y, Xie D, Shi B, Wang N, Li S. Flammability enhancement of swirling ammonia/air combustion using AC powered gliding arc discharges. Fuel 2021:122674. https://doi.org/10.1016/J.FUEL.2021.122674.
[31] Choe J, Sun W. Plasma assisted ammonia combustion: enhanced flame stability and reduced NOx emission. In: AIAA SCITECH 2022 Forum; 2022. https://doi.org/10.2514/6.2022-1452.
[32] Choe J, Sun W, Ombrello T, Carter C. Plasma assisted ammonia combustion: simultaneous NOx reduction and flame enhancement. Combust Flame 2021;228:430–2. https://doi.org/10.1016/j.combustflame.2021.02.016.
[33] Glassman I, Yetter RA, Glumac NG. Combustion. fifth ed. Waltham, Massachusetts: Academic Press; 2014.

[34] Starikovskaia SM. Plasma-assisted ignition and combustion: nanosecond discharges and development of kinetic mechanisms. J Phys D Appl Phys 2014;47. https://doi.org/10.1088/0022-3727/47/35/353001.
[35] Popov NA. Kinetics of plasma-assisted combustion: effect of non-equilibrium excitation on the ignition and oxidation of combustible mixtures. Plasma Sources Sci Technol 2016;25:043002. https://doi.org/10.1088/0963-0252/25/4/043002.
[36] Tsolas N, Lee JG, Yetter RA. Flow reactor studies of non-equilibrium plasma-assisted oxidation of n-alkanes. Philos Trans R Soc A Math Phys Eng Sci 2015;373:20140344. https://doi.org/10.1098/rsta.2014.0344.
[37] Lefkowitz JK, Guo P, Rousso A, Ju Y. Species and temperature measurements of methane oxidation in a nanosecond repetitively pulsed discharge. Philos Trans R Soc A Math Phys Eng Sci 2015;373:20140333. https://doi.org/10.1098/rsta.2014.0333.
[38] Stepanyan S, Minesi N, Tibere-Inglesse A, Salmon A, Stancu GD, Laux CO. Spatial evolution of the plasma kernel produced by nanosecond discharges in air. J Phys D Appl Phys 2019;52:295203. https://doi.org/10.1088/1361-6463/AB1BA4.
[39] Lefkowitz JK, Ombrello T. An exploration of inter-pulse coupling in nanosecond pulsed high frequency discharge ignition. Combust Flame 2017;180:136–47. https://doi.org/10.1016/J.COMBUSTFLAME.2017.02.032.
[40] Shen S, Laso I, Rozin N, Lefkowitz JK. On pulse energy and energy distribution for ignition of flowing mixtures. Proc Combust Inst 2022. https://doi.org/10.1016/J.PROCI.2022.07.008.
[41] Han X, Wang Z, He Y, Liu Y, Zhu Y, Konnov AA. The temperature dependence of the laminar burning velocity and superadiabatic flame temperature phenomenon for NH3/air flames. Combust Flame 2020;217:314–20. https://doi.org/10.1016/j.combustflame.2020.04.013.
[42] Lee JH, Kim JH, Park JH, Kwon OC. Studies on properties of laminar premixed hydrogen-added ammonia/air flames for hydrogen production. Int J Hydrogen Energy 2010;35:1054–64. https://doi.org/10.1016/J.IJHYDENE.2009.11.071.
[43] Zhong H, Shneider MN, Mao X, Ju Y. Dynamics and chemical mode analysis of plasma thermal-chemical instability. Plasma Sources Sci Technol 2021;30:035002. https://doi.org/10.1088/1361-6595/ABDE1C.
[44] Yi Y, Wang L, Guo H. Plasma-Catalytic decomposition of ammonia for hydrogen. Energy 2019:181–230. https://doi.org/10.1007/978-3-030-05189-1_7.